Magnetic structures of the Mn III weak ferromagnets $AMnF_4.H_2O$ (A=Rb and K)

1991 J. Phys.: Condens. Matter 3 2379

(http://iopscience.iop.org/0953-8984/3/14/017)

J. Phys.: Condens. Matter 3 (1991) 2379–2390. Printed in the UK

Magnetic structures of the Mn III weak ferromagnets $AMnF_4 \cdot H_2O$ (A = Rb and K)

Fernando Palacio†, Mercedes Andrés†, Juan Rodríguez-Carvajal‡ and Jean Pannetier‡

† Instituto de Ciencia de Materiales de Aragón, CSIC—Universidad de Zaragoza, E-50009 Zaragoza, Spain

‡ Institut Laue Langevin, Avenue des Martyrs, 156X F-38042 Grenoble Cédex, France

Received 26 July 1990, in final form 19 December 1990

Abstract. Neutron diffraction experiments on powder samples and single-crystal magnetization measurements are used to determine the magnetic structure of $KMnF_4 \cdot H_2O$ and $RbMnF_4 \cdot H_2O$. Both compounds order as antiferromagnets in the magnetic space group $C2'/c'$ ar, respectively, 8.3 K and 8.5 K. Their respective magnetic moments are located in the ac plane and deviates from strict antiparallelism by about 1.5°.

1. Introduction

Fluorinated Mn III compounds provide a fairly large variety of low-dimensional magnetic systems (see, for example [1–3] and references therein). Indeed, the influence of a strong Jahn–Teller (J-T) effect distorts the $[MnF_6]^{3-}$ group and favours a tendency to form chains or layers of corner-sharing coordination octahedra. Another consequence of the J-T distortion is to increase the single-ion anisotropy of the Mn^{3+} ions, therefore largely affecting the properties of these systems when they order magnetically. Thus, magnetic anisotropy is expected to be present and, accordingly, for an accurate understanding of the magnetic properties of these substances single-crystal measurements are required. This has been the case with $(NH_4)_2MnF_5$, for a long time the only Mn III derivative whose magnetism has been studied on single crystal. This substance has been described as a 1D Heisenberg antiferromagnet with weak ferromagnetic behaviour below (3D) ordering temperature [4].

We have recently reported on the magnetic properties of the compounds $AMnF_4 \cdot H_2O$, where A = Rb or K. AC magnetic susceptibility measurements on single crystals of these substances have shown that they are 1D Heisenberg antiferromagnets ordering as weak ferromagnets due to the existence of a small canting angle in the (antiparallel) alignment of their magnetic sublattices below T_c [5–7]. Both compounds crystallize in the monoclinic space group $C2/c$. The crystalline structure of these isomorphous materials consists of chains where alternate trans-$[MnF_4F_{2/2}]^{2-}$ and trans-$[MnF_2F_{2/2}(H_2O)_2]$ units are connected with each other by sharing apical fluorine atoms, as shown in figure 1 [6, 8, 9]. Superexchange paths along the chain consist of zigzag Mn–F–Mn bridges forming angles at the fluorine vertex of 137.2° and 138° for, respectively, the K and Rb compounds. The H atoms of the water molecule are involved in two

0953-8984/91/142379 + 12 $03.50

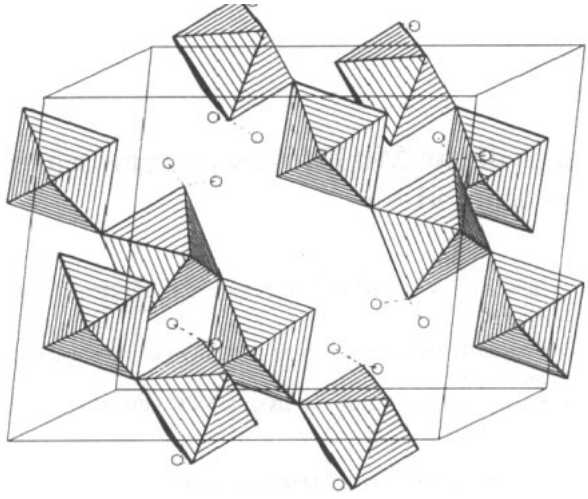

Figure 1. Room temperature crystal structure of $KMnF_4 \cdot H_2O$ projected on the *ac* plane. Dotted lines indicate hydrogen bonds.

hydrogen bonds. One is connecting two parallel chains of Mn–octahedra and shows a typical geometry. The other can be viewed as asymmetrically bifurcated and contributes to establish both inter- and intrachain links. From a magnetic point of view, the role the H bonds play is to transmit superexchange interactions between Mn ions of neighbour chains thus permitting the formation of a 3D magnetic structure. However, the number and nature of the magnetic sublattices in the structure cannot be established from susceptibility and magnetization measurements only; these measurements are also unable to unambiguously determine the magnetic symmetry of these materials. In addition, the existence of short-range order produces a tail in the spontaneous magnetization curve that makes uncertain the determination of T_c for about two degrees.

Therefore, we have performed neutron diffraction powder experiments as a function of the temperature in order to refine the nuclear structure, to calculate accurately the positions of the H atoms and to determine the (average) magnetic structure of each of the above mentioned compounds. We have also determined the dependence of the magnitude of the magnetic moment of each sublattice with the temperature. The presence of a small canting in the magnetic moments of the referred compounds requires complementary single-crystal magnetization measurements in order to establish precisely the direction of the magnetic moments within the crystal. Consequently, we also report on the magnetization measurements of these compounds. Some of these results have been briefly reported [7, 10].

2. Experimental section

The samples were prepared following already described methods [6, 8]. In order to deuterate the Rb derivative several recrystallizations in D_2O were performed. Since DF was not available, a small amount of HF was added instead in order to stabilize the oxidation state of the Mn III in the solution. As a result, the formula for the Rb

sample should be written as $RbMnF_4 \cdot [D_{(1-x)}H_x]_2O$; in addition, minor amounts of $RbMnF_4 \cdot H_2O$ were also found present in the sample, probably due to incomplete dissolution in one of the cycles of the recrystallization process. All the problems associated with deuteration were avoided in the case of the K derivative and completely undeuterated samples of $KMnF_4 \cdot H_2O$ were used. We found that the loss in precision, due to a higher background in the diffraction patterns because of incoherence, was largely compensated by a reduction in the number of the fitting parameters because only a single phase was present.

Diffraction patterns between 1.5 K and room temperature were taken in the diffractometer D1B at the Institute Laue Langevin (Grenoble). D1B is a high flux, medium resolution, powder diffractometer equipped with a 400-cell position-sensitive detector (PSD) spanning an angular range of 80° (2θ). The wavelength used was 2.52 Å. The limited angular range and the long wavelength precludes the refinement of individual temperature factors; therefore, only an overall temperature factor has been refined. A standard cryostat was used for the study of the sample as a function of temperature. A further pattern of 1.5 K of the undeuterated $RbMnF_4 \cdot H_2O$ was taken later on in the high resolution diffractometer D2B. In this case the neutron wavelength used was 1.5945 Å. This pattern permitted us to confirm the magnetic structure of this compound and to obtain an absolute value of the magnetic moment to scale those determined from the measurements of the partially deuterated sample on D1B.

The nuclear structure refinement was carried out using the programs available in the STRAP package [11]. The package is designed for automatic Rietveld refinement of large series of powder-diffraction patterns. For the analysis of the magnetic structures the Rietveld program [12], modified by A W Hewat [13], and FULLPROF program [14] were used.

Magnetization measurements were taken by integrating the emf induced in the two secondary coils of an AC susceptometer when the sample was moved from one to the other in the presence of a static uniform magnetic field produced in a superconducting coil [15]. A maximum magnetic field of 5 T was used in the experiments.

3. Neutron diffraction results

Powder diagrams of the $KMnF_4 \cdot H_2O$ in the temperature range between 5 K and 12 K and angular range of $17° \leqslant 2\theta \leqslant 75°$ are depicted in figure 2. The enhancement observed in some of the Bragg reflections corresponds to the magnetic ordering of the sample. The same behaviour is found for the Rb derivative. No additional magnetic peaks are observed to be present below T_c, therefore, for each compound the magnetic unit cell should be equal to the nuclear one, both unit cells being C centred.

The experiments made on a deuterated sample of the Rb derivative produced difficulties because of incomplete deuteration. Thus, to refine the nuclear structure at 100 K the composition formula $RbMnF_4 \cdot (H_{1-x}D_x)_2O$ was first considered yielding a R_F factor of 7.07%. Room temperature coordinates for the atomic positions were used as initial values in the refinement [8]. By assuming the presence of a small amount of a pure undeuterated phase of $RbMnF_4 \cdot H_2O$ in the sample the R_F factor was lowered down to 4.36%. For the calculation of the magnetic structure an indirect procedure was followed since the program used was not prepared to accept more than a single phase. A diffraction pattern made at 14 K, a temperature which was considered close to T_c but still well into the paramagnetic regime, was subtracted from a pattern made at 1.5 K.

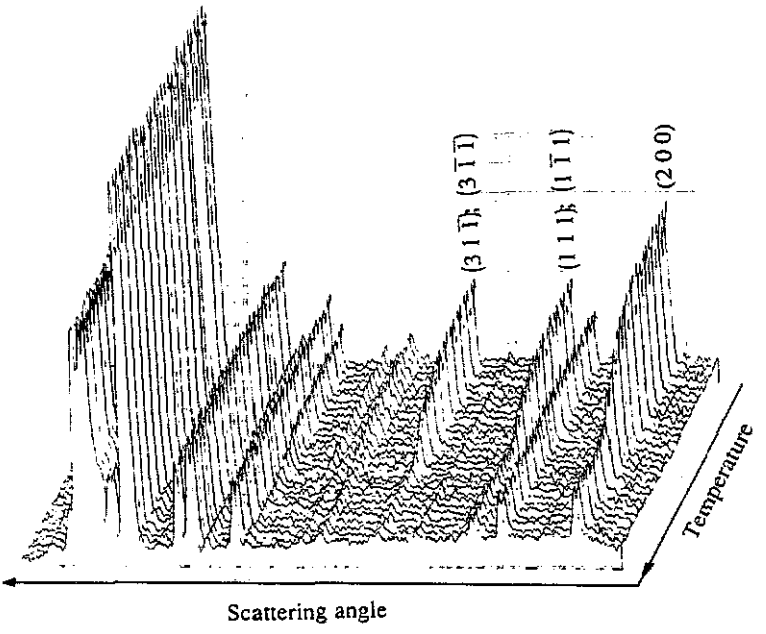

Figure 2. 3D plot of the powder diffraction patterns as a function of the temperature for $KMnF_4 \cdot H_2O$. The index of the peaks showing strong magnetic intensity are depicted.

The resulting difference pattern was assumed to be purely magnetic and only parameters corresponding to the orientation of the magnetic moments were fitted while the magnitude of the moments had to be left undetermined. The absolute value of such a magnitude was determined later on from a pattern of undeuterated $RbMnF_4 \cdot H_2O$ collected at 1.5 K.

The above difficulties were avoided in the case of the K derivative by using a pure undeuterated sample. The nuclear structure was refined from a pattern taken at 100 K and the (basic) magnetic structure was determined at 1.5 K using in both cases the Rietveld method. The starting structural parameters were taken from previously published x-ray determinations at room temperature [6].

Table 1. Unit cell parameters of $KMnF_4 \cdot H_2O$ and $RbMnF_4 \cdot H_2O$.

		300 K[a]	100 K	1.5 K
$KMnF_4 \cdot H_2O$	a (Å)	13.907(1)	13.781(3)	13.7546(14)
	b (Å)	6.2136(2)	6.160(1)	6.1406(5)
	c (Å)	10.492(1)	10.376(3)	10.3343(12)
	β (deg)	104.69(1)	104.42(1)	104.230(5)
$RbMnF_4 \cdot H_2O$	a (Å)	13.932(2)	13.859(2)[b]	13.8323(4)[c]
	b (Å)	6.471(1)	6.446(1)[b]	6.4285(2)[c]
	c (Å)	10.635(1)	10.492(1)[b]	10.4837(3)[c]
	β (deg)	104.54(1)	104.204(6)[b]	103.980(2)[c]

[a] As taken from [5] and [8].
[b] The data corresponds to the partially deuterated sample.
[c] Parameters fitted from the pattern made in the high resolution diffractometer D2B.

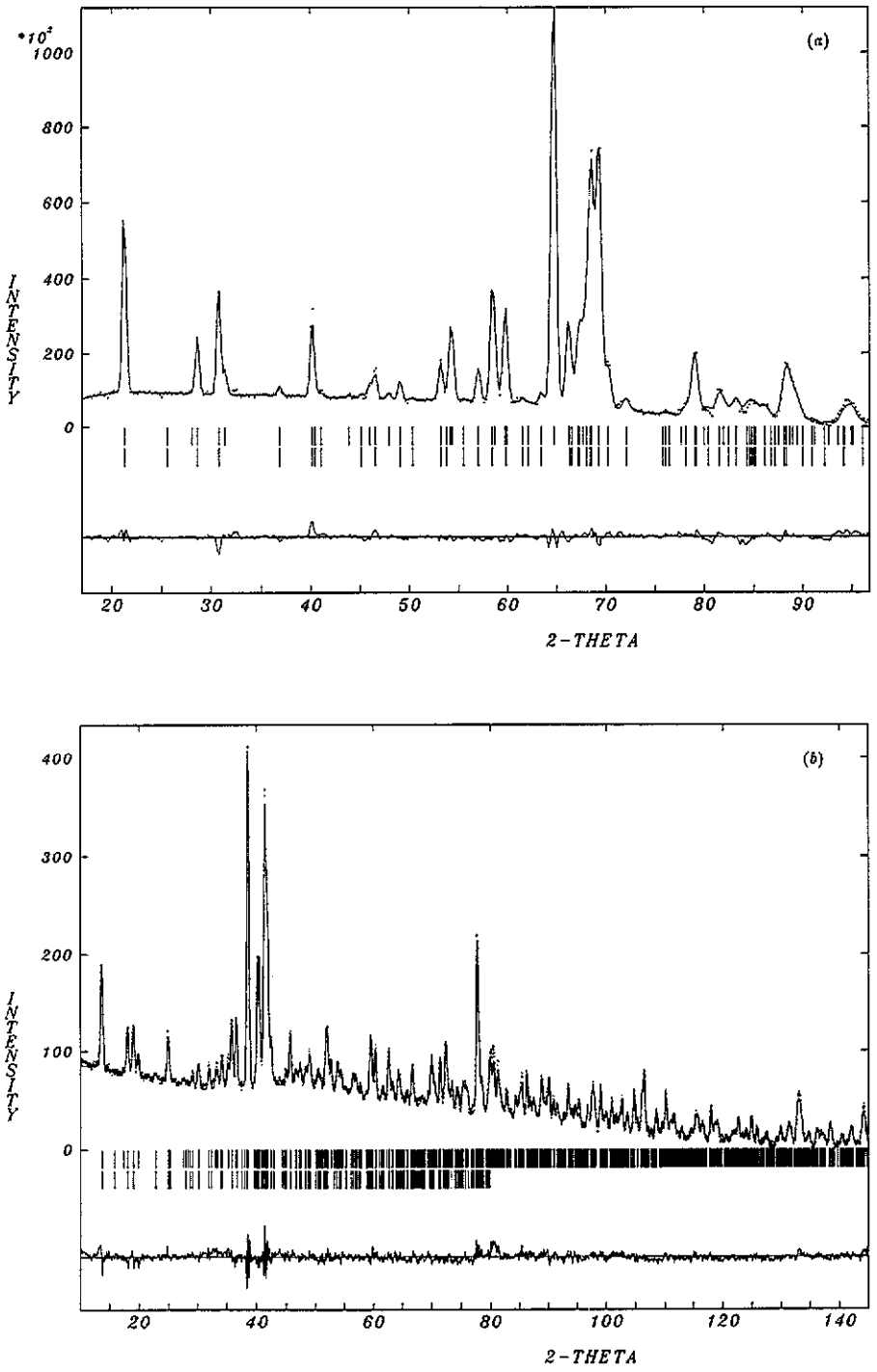

Figure 3. Observed (+) and calculated (full line) pattern at 1.5 K of: (*a*) $KMnF_4 \cdot H_2O$, from D1B, and (*b*) $RbMnF_4 \cdot H_2O$, from D2B. Angular positions of the allowed Bragg reflections are indicated by small bars as explained in the text. The difference pattern $y_{obs} - y_{calc}$ is given at the bottom of the figure.

Table 2. Structural parameters of $KMnF_4 \cdot H_2O$ and $RbMnF_4 \cdot H_2O$ at 1.5 K.

	x/a	*y/b*	*z/c*
$KMnF_4 \cdot H_2O$ (D1B; λ = 2.52 Å)			
K	0.0797(14)	0.7218(50)	0.4396(22)
Mn(1)	1/4	1/4	1/2
Mn(2)	0	0.2456(73)	1/4
F(1)	0.1023(10)	0.2451(35)	0.4370(14)
F(2)	0.2484(12)	−0.0466(27)	0.4608(14)
F(3)	0.0665(12)	0.0425(25)	0.1821(14)
F(4)	0.0734(16)	0.4630(26)	0.1871(15)
O	0.2615(16)	0.3331(38)	0.3016(21)
H(1)	0.1959(24)	0.4045(48)	0.2505(25)
H(2)	0.3095(27)	0.4029(51)	0.2920(30)
$RbMnF_4 \cdot H_2O$ (D2B; λ = 1.5945 Å)			
Rb	0.0790(2)	0.7452(10)	0.4388(3)
Mn(1)	1/4	1/4	1/2
Mn(2)	0	0.2456(24)	1/4
F(1)	0.1051(3)	0.2510(12)	0.4344(4)
F(2)	0.2494(4)	−0.0263(7)	0.4584(4)
F(3)	0.0707(4)	0.0441(10)	0.1874(6)
F(4)	0.0715(5)	0.4498(10)	0.1883(5)
O	0.2647(5)	0.3311(9)	0.3086(6)
H(2)	0.2097(7)	0.3935(14)	0.2508(11)
H(1)	0.3199(8)	0.4131(16)	0.3070(10)

Table 1 shows the relevant crystallographic fitted parameters and the reliability factors at 1.5 K and 100 K for the K and Rb derivatives. The most significant interatomic distances and angles at 1.5 K are shown in table 2 for both compounds. The Rietveld refinement of the nuclear and magnetic structure of $KMnF_4 \cdot H_2O$ and $RbMnF_4 \cdot H_2O$ at 1.5 K are shown in figure 3 where the observed, calculated and difference patterns and the Bragg reflection markers have been plotted. The second row of Bragg reflection markers corresponds to the magnetic structure. For the refinement of the structure of the Rb derivative the high resolution data from the D2B diffractometer has been used. In this case only reflections up to $2\theta = 80°$ were considered in the refinement of the magnetic part, since the magnetic form factor rends negligible magnetic intensities at higher angles.

4. Magnetization results

For the magnetization measurements a well-shaped single crystal of each respective compound was selected. The crystals were oriented along a direction parallel to the weak ferromagnetic axis. The measurements were made as a function of magnetic field and at a variety of temperatures. After every run at a temperature below T_c the sample was heated up to the paramagnetic state and then with zero field cooled down to the next selected temperature. As the magnetic field increases the magnetization curves show first the saturation of the weak ferromagnetic moments and from there a linear increase characteristic of the antiferromagnetic regime is observed. No field-induced magnetic

phase transition has been observed up to the maximum magnetic field of 5 T available in these experiments. The lower magnetic field region of the magnetization curves is depicted in figures 4(*a*) and (*b*) for, respectively, $KMnF_4 \cdot H_2O$ and $RbMnF_4 \cdot H_2O$. In both compounds the saturation of the weak ferromagnetic moments is observed to occur at rather low magnetic fields; this is clearly shown in figure 5 where the representative hysteresis cycle of the K derivative measured at 4.2 K is given.

The temperature dependence of the spontaneous magnetization, as represented in figure 6, has been derived by extrapolating for each temperature in the magnetization curves the saturation of the ferromagnetic moment down to H = 0 Oe. The magnitude of the spontaneous (weak) ferromagnetic moment, $M_S(0)$, has been calculated by extrapolating the temperature dependence of the spontaneous magnetization down to $T = 0$ K. Values of $M_S(0) = 625$ emu.Oe/mol (0.11 μ_B) and 675 emu.Oe/mol (0.12 μ_B) have been calculated for, respectively, $KMnF_4 \cdot H_2O$ and $RbMnF_4 \cdot H_2O$. From the simple relation $\gamma = tg^{-1}[M_S(0)/Ng\mu_B S]$ the canting angle is calculated to be $\gamma = 1.5°$ and 1.7° for the K and Rb derivatives.

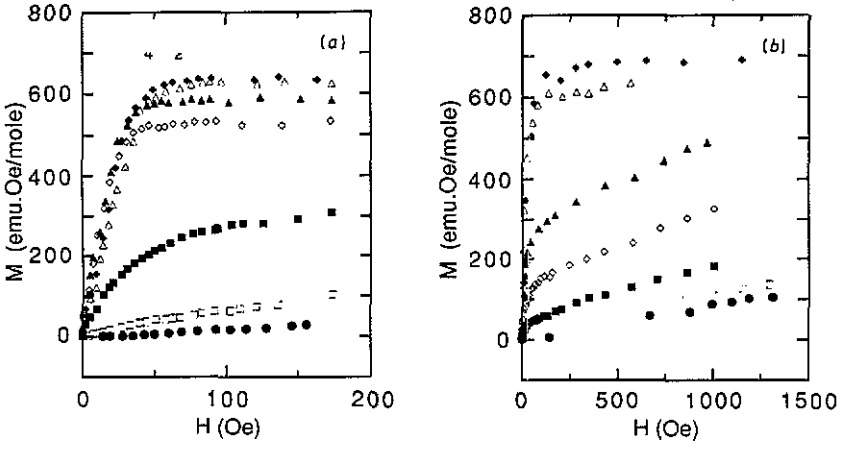

Figure 4. Magnetization curves as a function of the magnetic field of: (*a*) $KMnF_4 \cdot H_2O$: 4.2 K (♦); 5.0 K (△); 7.5 K (▲); 8.0 K (◊); 8.5 K (■); 9.0 K (□); 9.5 K (●), and (*b*) $RbMnF_4 \cdot H_2O$: 4.2 K (♦); 6.0 K (△); 7.6 K (▲); 8.1 K (◊); 8.7 K (■); 9.5 K (□); 10.0 K (●).

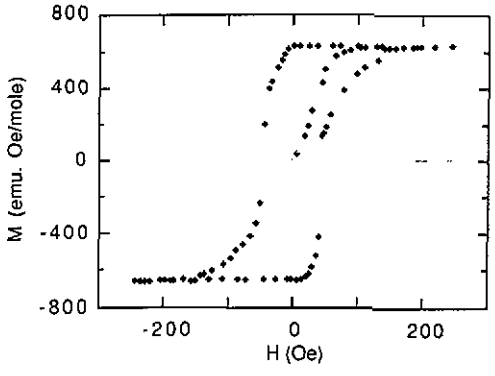

Figure 5. Hysteresis cycle at 4.2 K for $KMnF_4 \cdot H_2O$.

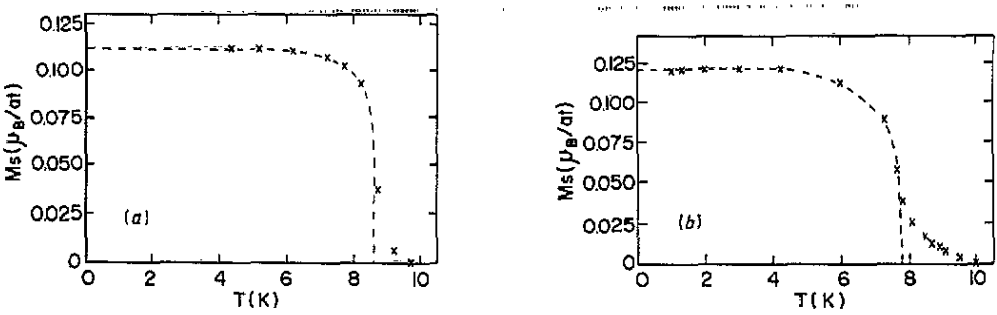

Figure 6. Temperature dependence of the spontaneous magnetization of: (*a*) $KMnF_4 \cdot H_2O$; (*b*) $RbMnF_4 \cdot H_2O$.

5. Discussion

Cell-constrained profile refinement was used to analyse the evolution of the integrated intensities as a function of the temperature [11]. In figure 7 such evolution is shown for the Rb derivative. The dependence of the magnitude of the magnetic moment of each sublattice with the temperature has been calculated by means of magnetic structure refinement. Figure 8 shows the sublattice magnetization of both K and Rb derivatives as a function of the temperature. From figures 7 and 8 one can determine that magnetic ordering occurs at about 8.3 K and 8.5 K for, respectively, the K and Rb derivatives. These temperatures compare quite well with the respective values of 8.45 K and 8.9 K which correspond to the temperatures where the peak in the susceptibility curve appears [5, 6]. It is worth noting that in the $RbMnF_4 \cdot H_2O$ the shape of the AC susceptibility curve measured in the direction parallel to the weak ferromagnetic moment exhibits a complicated pattern of three peaks at 8.9, 7.8 and 7.3 K, thus making very uncertain the determination of T_c.

In order to solve the magnetic structures it is necessary to take into account all the information about the symmetry and the magnetic properties of these systems. First of all, the crystalline structures of both K and Rb derivatives do not change in the range of temperature studied. The point symmetry at the Mn sites is $\bar{1}$ and 2, respectively for Mn(1) and Mn(2). The centre of symmetry $\bar{1}$ does not constrain the direction of the magnetic moments of the Mn(1) ions; however, the 2-fold axis forces the magnetic moments of the Mn(2) ions to be oriented either parallel to the $\vec{b}$ axis, in which case the

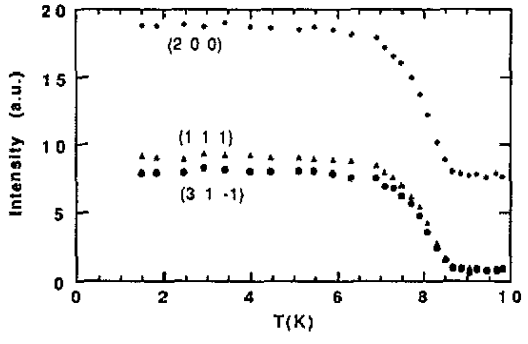

Figure 7. Integrated intensities of a series of Bragg reflections with large magnetic contribution as a function of the temperature. The data correspond to $RbMnF_4 \cdot H_2O$.

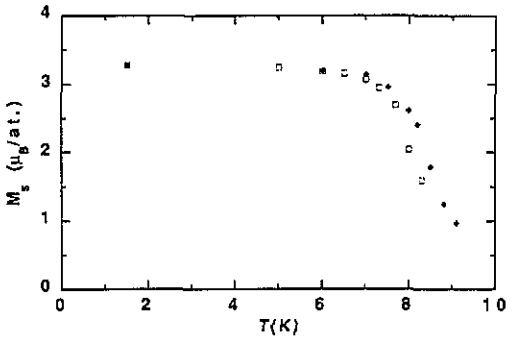

Figure 8. Temperature dependence of the staggered magnetization of $KMnF_4 \cdot H_2O$ (□) and $RbMnF_4 \cdot H_2O$ (♦).

magnetic point symmetry is 2, or perpendicular to the $\bar{b}$ axis, in which case the point symmetry is $2'$. In the second case the magnetic moments do not point *a priori* along any direction within the referred plane. Magnetic susceptibility data are consistent with the second option for Mn(2), since the direction of the moments is restricted to the *ac* plane [5, 6]. Moreover, the analysis of the magnetic susceptibility data gives negative values for the superexchange interactions Mn(1)–F–Mn(2). As a consequence, the magnetic moments of the Mn^{3+} ions should be of the form

$$\mu[\mathrm{Mn}(1)] = (\mu_x, 0, \mu_z)$$
$$\mu[\mathrm{Mn}(2)] = (-\mu_x, 0, -\mu_z).$$

In order to determine the rotation of the moments for the rest of the equivalent positions in the unit cell, the simple consideration that the magnetic cell is the same as the nuclear one implies that the glide plane c should actually be c'. In other words, the spin direction should not be inverted through the glide reflection.

To get a deeper insight into the nature of the magnetic couplings allowed by symmetry, we have performed a theoretical group analysis of the possible magnetic structures. Using the Bertaut method [16] we have obtained the representations of the space group $C2/c$ for an integral wave vector. The basis functions corresponding to the two Mn(1) and Mn(2) sites have been obtained and a summary is given in table 3.

As the two sites are coupled via antiferromagnetic superexchange interaction, the spin arrangement corresponding to Mn(1) and Mn(2) must belong to the same representation. Since the magnetic cell is centred, the character of the translation $t = [1/2\ 1/2\ 0]$ must be $+1$, therefore the only representations allowed are $\Gamma_{1g}(++)$ and $\Gamma_{3g}(-+)$. The $\Gamma_{1g}(++)$ representation for the Mn(1) site implies a ferromagnetic structure with magnetic moments along the b axis which is in contradiction with the fact that, as stated above, magnetic susceptibility data support magnetic moments lying in the *ac* plane. Therefore, the representation of the magnetic structure should be $\Gamma_{3g}(-+)$. The magnetic space group corresponding to this one-dimensional representation is $C2'/c'$. In these conditions, the most general magnetic structure is consistent with the following spin arrangement:

$$\Gamma_{3g}(-+)^{(1)}(F_x^{(1)}, G_y^{(1)}, F_z^{(1)})$$
$$\Gamma_{3g}(-+)^{(2)}(F_x^{(2)}, 0, F_z^{(2)}).$$

In principle the existence of a G_y component on the Mn(1) sites and even differences in the amplitude of the magnetic moments of the two sites are permitted by symmetry.

Table 3. Representations of the $C2/c$ space group for propagation vector $k = 0$ and basis vectors corresponding to the two sites Mn(1) and Mn(2) and describing the possible magnetic structures. The notation used here corresponds to the symbols in [23]. The magnetic modes are defined as:

$$F = S_1 + S_2 + S_3 + S_4, G = S_1 - S_2 + S_3 - S_4, C = S_1 + S_2 - S_3 - S_4, A = S_1 - S_2 - S_3 + S_4$$

where S_i is the 'spin' (axial vector) of the sublattice i of a given site. The representations are labelled by the symbol Γ with a numerical subscript and g or u for representations in which the character of the inversion is $+1$ or -1, respectively. Between parentheses we give the characters of the two remaining generators 2_y and t.

Numbering of the Bravais sublattices corresponding to the sites Mn(1) and Mn(2):

Mn(1): (4d)	−1	$(1/4\ 1/4\ 1/2)^1$	$(3/4\ 1/4\ 0)^2$	$(3/4\ 3/4\ 1/2)^3$	$(1/4\ 3/4\ 0)^4$
Mn(2): (4e)	2	$(0\ y\ 1/4)^1$	$(0\ -y\ 3/4)^2$	$(1/2\ 1/2\ +y\ 1/4)^3$	$(1/2\ 1/2\ -y\ 3/4)^4$

Generators of the factor group: $2_y(0\ y\ 1/4)$, $t[1/2\ 1/2\ 0]$ and $-1(000)$

	Mn(1)			Mn(2)		
	x	y	z	x	y	z
$\Gamma_{1g}(++)$	G_x	F_y	G_z	—	F_y	—
$\Gamma_{2g}(+-)$	—	—	—	—	C_y	—
$\Gamma_{3g}(-+)$	F_x	G_y	F_z	F_x	—	F_z
$\Gamma_{4g}(--)$	—	—	—	C_x	—	C_z
$\Gamma_{1u}(++)$	—	—	—	—	G_y	—
$\Gamma_{2u}(+-)$	A_x	C_y	A_z	—	A_y	—
$\Gamma_{3u}(-+)$	—	—	—	G_x	—	G_z
$\Gamma_{4u}(-+)$	C_x	A_y	C_z	A_x	—	A_z

This second possibility would imply ferrimagnetic behaviour. Susceptibility measurements are consistent with the existence of a small canted antiferromagnetic structure (weak ferromagnetism), therefore one can assume an equal value for the magnetic moments of the two sites: μ[Mn(1)] = μ[Mn(2)]. This assumption does not constrain the magnetic moments of the two sites to be parallel. In fact the Shubnikov group $C2'/c'$ is a 'ferromagnetic group' [17], therefore, it allows the presence of a weak ferromagnetic component as the result of a canting of the spins of a sublattice with respect to the other. The small canting angle of the two magnetic sublattices observed in the magnetic measurements is far below the resolution of our neutron powder diffraction data. For this reason we have constrained our refinement to an exact antiparallelism between the spins of the two sublattices as represented in figure 9 for the Rb derivative.

The above approximation to the magnetic structure has two degrees of freedom which correspond to the direction of the spins within the plane and to the magnitude of the magnetic moment. The magnetic moment of each sublattice is, in the case of the K derivative, 3.2 μ_B at 1.5 K and the angle of the spin direction with respect to the chain axis, [101], is about 44°; for the case of the Rb derivative we obtain 3.3 μ_B and 38°. The direction of the magnetic moments had been previously assumed to be perpendicular to the chain direction on the basis of comparing the external morphology of a small crystal oriented in a diffractometer with that of the large ones used in the magnetic measurements. This assumption was only used to assign an orientation to the principal axis of the susceptibility tensor within the *ac* plane.

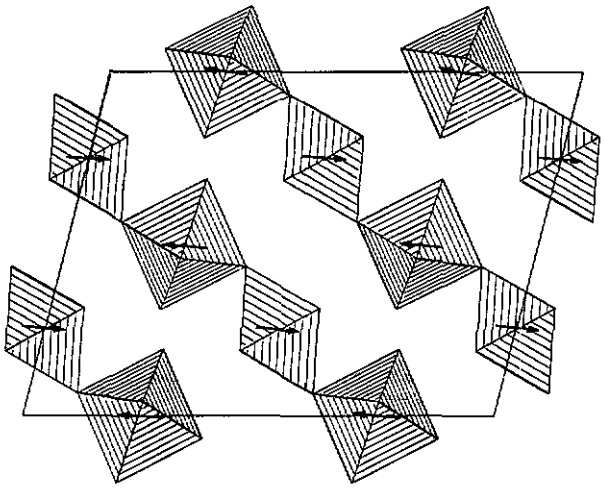

Figure 9. Magnetic structure projected on the *ac* plane with the orientations of the moments corresponding to $RbMnF_4 \cdot H_2O$.

The actual spin direction and the small canting angle between the spins of the two sites, can be understood as a result of the competition between the single-ion anisotropy of the Mn III in each octahedral site. The main isotropic exchange interaction J [Mn(1)–Mn(2)] does not impose any particular direction of the magnetic moments with respect to the crystalline frame. This interaction tends just to keep the spins exactly antiparallel. The elongated axis of the two types of octahedra are not parallel and one can expect that terms of the form $D_1(\boldsymbol{u}_1\boldsymbol{S}_1)^2$ and $D_2(\boldsymbol{u}_2\boldsymbol{S}_2)^2$ are present in the Hamiltonian, D_1 and D_2 being the strength of the single-ion anisotropy and $\boldsymbol{u}_1$ and $\boldsymbol{u}_2$ the unit vectors along the directions of anisotropy in the sites Mn(1) and Mn(2), respectively. The competition between the isotropic exchange and the single-ion anisotropy is, therefore, a plausible mechanism that can explain the presence of a weak ferromagnetic component in this compound. Of course antisymmetric (Dyalozynski–Moriya) and anisotropic exchange terms are not excluded by symmetry and can also contribute to the actual magnetic structure of these compounds.

Acknowledgment

The research in Zaragoza has been supported by grant MAT88-0174, from the Comisión Interministerial de Ciencia y Tecnología.

References

[1] Köhler P, Massa W, Reinen D, Hoffman B and Hoppe R 1978 *Z. Anorg. (Allg.) Chem.* **446** 131
[2] Núñez P, Darriet J, Bukovec P, Tressaud A and Hagenmuller P 1987 *Mat. Res. Bull.* **22** 661
[3] Pebler J, Massa W, Lass H and Ziegler B 1987 *J. Solid State Chem.* **71** 87
[4] Kida J and Watanabe T 1973 *J. Phys. Soc. Japan* **34** 952
[5] Palacio F, Andrés M, Horne R and van Duyneveldt A J 1986 *J. Magn. Magn. Mater.* **54–57** 1487

[6] Palacio F, Andrés M, Esteban-Calderón C, Martínez-Ripoll M and García-Blanco S 1988 *J. Solid State Chem.* **76** 33
[7] Palacio F, Andrés M, van Noort D and van Duyneveldt A J 1988 *J. Physique* **49**(12) C8–819
[8] Kaucic V and Bukovec P 1979 *J. Chem. Soc. Dalton Trans.* 1512
[9] Massa W, Baum G and Drueeke S 1988 *Acta Crystallogr.* C **44** 167
[10] Palacio F, Andrés M, Rodríguez-Carvajal J and Pannetier J 1989 *Proc. 9th. Gen. Conf. Cond. Mat. Div. of the E.P.S. (Europhys. Conf. Abstracts 13A)* ed J P Laheurte, M le Bellac and F Raymond p 231
[11] Rodriguez J, Anne M and Pannetier J *ILL Internal report* 87Ro14T
[12] Rietveld H M 1969 *J. Appl. Cryst.* **2** 65
[13] Hewat A W 1973 *Harwell Report* AERE-R7350
[14] Rodríguez-Carvajal J unpublished
[15] Rillo C 1986 *Universidad de Zaragoza Report* TSNA86
[16] Bertaut E F 1968 *Acta Cryst.* A **24** 217; 1963 Spin Configuration of Ionic Structures: Theory and Practice *Magnetism* ed G T Rado and H Suhl, vol 3 (New York: Academic) p 150
[17] Opechovski W and Guccione R 1965 *Magnetism* vol IIA, ed G T Rado and H Suhl (New York: Academic) p 105